J|A|C|S ARTICLES

Published on Web 04/27/2010

Semiconductor Nanocrystals Functionalized with Antimony Telluride Zintl Ions for Nanostructured Thermoelectrics

Maksym V. Kovalenko,*[,†] Boris Spokoyny,[†] Jong-Soo Lee,[†] Marcus Scheele,[‡] Andrew Weber,[†] Susanthri Perera,[§] Daniel Landry,[§] and Dmitri V. Talapin*[,†,||]

Department of Chemistry, University of Chicago, Illinois 60637, The Molecular Foundry, Lawrence Berkeley National Laboratory, Berkeley, California 94720, Evident Technologies Inc., Troy, New York 12180, Center for Nanoscale Materials, Argonne National Lab, Argonne, IL 60439

Received November 11, 2009; E-mail: mvkovalenko@uchicago.edu; dvtalapin@uchicago.edu

Abstract: The energy efficiency of heat engines could be improved by the partial recovery of waste heat using thermoelectric (TE) generators. We show the possibility of designing nanostructured TE materials using colloidal inorganic nanocrystals functionalized with molecular antimony telluride complexes belonging to the family of Zintl ions. The unique advantage of using Zintl ions as the nanocrystal surface ligands is the possibility to convert them into crystalline metal chalcogenides, thus linking individual nanobuilding blocks into a macroscopic assembly of electronically coupled functional modules. This approach allows preserving the benefits of nanostructuring and quantum confinement while enabling facile charge transport through the interparticle boundaries. A developed methodology was applied for solution-based fabrication of nanostructured n- and p-type $Bi_{2-x}Sb_xTe_3$ alloys with tunable composition and $PbTe-Sb_2Te_3$ nanocomposites with controlled grain size. Characterization of the TE properties of these materials showed that their Seebeck coefficients, electrical and thermal conductivities, and ZT values compared favorably with those of previously reported solution-processed TE materials.

1. Introduction

Thermoelectric (TE) energy conversion is a very attractive method for environmentally benign cooling and for recovering energy from a waste heat. The limited presence of TE devices on the marketplace is mainly the result of low thermoelectric figures of merit (ZT) for known TE materials. A practical TE material should combine high Seebeck coefficient (S, also known as thermopower), high electrical conductivity (σ), and low thermal conductivity (κ): $ZT = S^2\sigma T/\kappa$, where T is the absolute temperature. The power factor $P = S^2\sigma$ determines the electric power that can be generated by a given TE material.[1]

Bismuth telluride (Bi_2Te_3) based alloys are among the most studied TE materials. They produce $ZT \approx 1$ and efficiencies $\sim$10% of the Carnot limit, whereas $ZT \approx 4$ is required for a TE device that is competitive with alternative technologies such as combustion engines and compressor-based refrigerators.[2−4] To overcome the limitations of bulk semiconductors, the focus of TE research has recently shifted toward low-dimensional materials.[3,5−7] The expectations originate from (i) the reduction of lattice thermal conductivity due to phonon scattering at the grain boundaries, without significant deterioration of electrical conductivity (i.e., the concept of "electron crystal−phonon glass")[8] and (ii) the increase of S and correspondingly of the power factor $S^2\sigma$ due to quantum confinement[9,10] or through energy filtering.[11,12] Humphrey and Linke derived the conditions under which reversible diffusive electron transport could be achieved in nanostructured TE materials.[13] Harman et al. observed $ZT \approx 1.6$ in a $PbSe_xTe_{1-x}$ based quantum dot superlattice grown by molecular beam epitaxy (MBE);[14] Venkatasubramanian et al. reported $ZT \approx 2.4$ in a p-type MBE-grown Bi_2Te_3/Sb_2Te_3 superlattice.[15] These studies provided a proof of principle, but their practical use was hampered by complicated and expensive fabrication techniques. The technological future of TE materials lies in the ability to fabricate "bulk" nanostructured TE materials in scalable quantities (kilograms or even tons). Important steps toward cost-effective nanostructured TE materials were reported by the Kanatzidis group, who prepared n-type $AgPb_mSbTe_{2+m}$ (LAST)[16] and p-type $Na_{0.95}Pb_{20}SbTe_{22}$ (SALT)[17] by high-temperature solid-state synthesis, yielding ZT values of $\sim$1.7 and $\sim$1.6, respec-

[†] University of Chicago.
[‡] Lawrence Berkeley National Laboratory.
[§] Evident Technologies Inc.
[||] Center for Nanoscale Materials.

(1) Snyder, G. J.; Toberer, E. S. *Nat. Mater.* **2008**, *7*, 105–114.
(2) Vining, C. B. *Nat. Mater.* **2009**, *8*, 83–85.
(3) *Thermoelectrics Handbook: Macro to Nano*; Rowe, D. M., Ed.; CRC Press: Boca Raton, FL, 2006.
(4) Snyder, G. J.; Toberer, E. S. *Nat. Mater.* **2008**, *7*, 105–114.
(5) Tritt, T. M. *Science* **1996**, *272*, 1276–1277.
(6) Hochbaum, A. I.; Chen, R.; Delgado, R. D.; Liang, W.; Garnett, E. C.; Najarian, M.; Majumdar, A.; Yang, P. *Nature* **2008**, *451*, 163–167.
(7) Sales, B. C. *Science* **2002**, *295*, 1248–1249.
(8) *CRS Handbook on Thermoelectrics*; Rowe, D. M., Ed.; CRC Press: Boca Raton, FL, 1995.
(9) Hicks, L. D.; Dresselhaus, M. S. *Phys. Rev. B* **1993**, *47*, 12727.
(10) Hicks, L. D.; Dresselhaus, M. S. *Phys. Rev. B* **1993**, *47*, 16631.
(11) Vashaee, D.; Shakouri, A. *Phys. Rev. Lett.* **2004**, *92*, 106103.
(12) Heremans, J. P.; Thrush, C. M.; Morelli, D. T. *Phys. Rev. B* **2004**, *70*, 115334.
(13) Humphrey, T. E.; Linke, H. *Phys. Rev. Lett.* **2005**, *94*, 096601.
(14) Harman, T. C.; Taylor, P. J.; Walsh, M. P.; LaForge, B. E. *Science* **2002**, *297*, 2229–2232.
(15) Venkatasubramanian, R.; Siivola, E.; Colpitts, T.; O'Quinn, B. *Nature* **2001**, *413*, 597–602.

 10.1021/ja909591x

tively. High *ZT* values originated from unusually low thermal conductivity caused by nanoscale inclusions spontaneously formed in the host material during crystallization. In 2008 Poudel et al. reported that simple grinding of bulk $(Bi,Sb)_2Te_3$ ingots followed by hot-pressing the nanoscale grains back into a pellet produced a material with $ZT \approx 1.4$ at 100 °C,[18] which is the record number for $(Bi,Sb)_2Te_3$. The same group later extended this approach to p-SiGe, demonstrating 50% increase in *ZT* up to ~0.95 at 800 °C.[19]

Thin-film TE generators using 30−100 μm thick semiconductor layers allow for a high power density per unit area combined with light weight,[20] given that an efficient heat sink is provided. At the same time, it is technologically challenging to fabricate such devices from bulk crystals obtained via conventional solid-state synthesis of TE semiconductors. In this case, solution deposition of the TE material might be very convenient, especially for nonplanar geometries such as a wall of engine combustion chamber. Furthermore, solution-deposited thin film TE materials can also find several important niche applications, such as temperature sensors using Seebeck voltage readouts[21] and integrated microdevices. Microintegrated Peltier devices (microcoolers) used to stabilize thermally sensitive components in microelectronics, lasers, and infrared detectors[22,23] would require ~1−10 μm thick films deposited on insulating substrates and patterned by conventional lithography and etching. The possibility of low-temperature solution deposition is also very attractive for manufacturing such devices on flexible substrates such as Kapton polyimide.[24] These small TE devices can also perform opposite functions if used as microgenerators for low-power applications such as hearing aids and wristwatches.

Semiconductor nanocrystals (NCs) with precisely tailored size and shape are promising candidates for nanostructured TE semiconductors.[25] The phonon scattering can be optimized by controlling grain sizes, interfaces, and chemical compositions. At the same time, reported efforts to make TE materials from chemically synthesized NCs revealed serious challenges mainly associated with the presence of organic molecules (surface ligands) at the NC surface. Being vitally important for NC synthesis, these ligands are highly insulating and hamper electrical conductivity of NC solids. The crude removal of surface ligands by thermal treatments usually leaves carbonaceous residues[26] or chemical impurities behind, creating midgap trap states[27] or leading to NC sintering.[28] As a relevant example, colloidal thiol-capped Bi_2Te_3 NCs, 2.5−10 nm in size, generated an undesired Bi_2Te_2S phase with modest TE characteristics upon annealing.[29] Dirmyer et al. prepared Bi_2Te_3 nanostructured material without detectable amounts of Bi_2Te_2S by annealing larger, 20−100 nm, thiol-capped Bi_2Te_3 NCs[30] and, to the best of our knowledge, provided the first detailed characterization of colloidally prepared Bi_2Te_3 TE materials. Very recently, Scheele et al. reported a preparation of n-type Bi_2Te_3 pellets from colloidal NCs with $ZT \approx 0.2$ at room temperature[31] and Wang et al. reported solution-processable precursors to bismuth chalcogenides with $ZT \approx 0.4$.[32] We found no relevant references on designing bismuth−antimony−telluride $(Bi,Sb)_2Te_3$, which is the workhorse material for TE cooling applications, from colloidal NCs.

We have recently developed a novel, generalized approach to create all-inorganic NC solids by the complete replacement of organic ligands with inorganic molecular metal chalcogenide complexes (MCCs).[33] Acting as an "electronic glue", MCC ligands greatly improved interparticle charge transport in metallic and semiconducting NC solids. Furthermore, MCCs themselves can be used as the precursors for a high-purity semiconductor phase.[34] Here we employ this new surface chemistry for fabricating nanostructured PbTe, Bi_2Te_3, and Sb_2Te_3 phases known as superior TE materials.[3] In the first approach, antimony telluride Zintl ions (further referred to as Sb_2Te_3-MCCs) are used as the capping ligands for monodisperse PbTe NCs. In the second approach, we perform solid-state chemical transformation to convert sulfide NC precursors into telluride nanocomposite material via S^{2-}-to-Te^{2-} anion exchange, e.g., by reacting Sb_2Te_3-MCCs containing excessive Te with PbS or Bi_2S_3 NCs. Single-phase $(Bi, Sb)_2Te_3$ alloys and biphase $PbTe/Sb_2Te_3$ were prepared using this approach. We demonstrate high electrical conductivity, high Seebeck coefficients, and control over p- and n-type doping for $(Bi,Sb)_2Te_3$ thin films.

2. Experimental Section

Chemicals. All manipulations were carried out using standard Schlenk line techniques and nitrogen-filled gloveboxes. Oleic acid (OA, technical grade, Aldrich), bismuth(III) acetate ($BiAc_3$, 99.99%, Aldrich), lead acetate trihydrate ($PbAc_2 \cdot 3H_2O$, Aldrich), squalane (99%, Aldrich), 1-octadecene (ODE, 90%, Aldrich), trioctylphosphine (TOP, 97%, Strem), antimony(III) telluride (99.999%, Alfa), tellurium (shot, 99.999%, Aldrich), sulfur (99.998%, Aldrich), dimethyl sulfoxide (anhydrous, 99.9%, Aldrich), hydrazine (anhydrous, 98%, Aldrich), acetonitrile (anhydrous, 99.8%, Aldrich), and hexane (anhydrous, 95%, Aldrich) were used as received.

Synthesis of Sb_2Te_3-MCCs and Sb_2Se_3-MCC. Finely ground Sb_2Te_3 (250 mg, 0.4 mmol) and a 4-fold molar excess of Te (1.6 mmol, 204 mg) were dissolved in N_2H_4 (10 mL) inside a glovebox,

(16) Hsu, K. F.; Loo, S.; Guo, F.; Chen, W.; Dyck, J. S.; Uher, C.; Hogan, T.; Polychroniadis, E. K.; Kanatzidis, M. G. *Science* **2004**, *303*, 818–821.
(17) Pierre, F. P.; Poudeu, J. D.; Adam, A.; Downey, D.; Jarrod, L.; Short, J. L.; Hogan, T. P.; Kanatzidis, M. G. *Angew. Chem., Int. Ed.* **2006**, *45*, 3835–3839.
(18) Poudel, B.; Hao, Q.; Ma, Y.; Lan, Y.; Minnich, A.; Yu, B.; Yan, X.; Wang, D.; Muto, A.; Vashaee, D.; Chen, X.; Liu, J.; Dresselhaus, M. S.; Chen, G.; Ren, Z. *Science* **2008**, *320*, 634–638.
(19) Joshi, G.; Lee, H.; Lan, Y.; Wang, X.; Zhu, G.; Wang, D.; Gould, R. W.; Cuff, D. C.; Tang, M. Y.; Dresselhaus, M. S.; Chen, G.; Ren, Z. *Nano Lett.* **2008**, *8*, 4670–4674.
(20) Mayer, P. M.; Ram, R. J. *Nanoscale Microscale Thermophys. Eng.* **2006**, *10*, 143–155.
(21) Rajasekar, K.; Kungumadevi, L.; Subbarayan, A.; Sathyamoorthy, R. *Ionics* **2008**, *14*, 69–72.
(22) Shafai, C.; Brett, M. J. *J. Vac. Sci. Technol. A* **1997**, *15*, 2798–2801.
(23) Zou, H. L.; Rowe, D. M.; Williams, S. G. K. *Thin Solid Films* **2002**, *408*, 270–274.
(24) Goncalves, L. M.; Rocha, J. G.; Couto, C.; Alpuim, P.; Min, G.; Rowe, D. M.; Correia, J. H. *J. Micromech. Microeng.* **2007**, *17*, S168–S173.
(25) Talapin, D. V.; Lee, J.-S.; Kovalenko, M. V.; Shevchenko, E. V. *Chem. Rev.* **2010**, 389–458.
(26) Drndic, M.; Jarosz, M. V.; Morgan, N. Y.; Kastner, M. A.; Bawendi, M. G. *J. Appl. Phys.* **2002**, *92*, 7498–7503.
(27) Kuno, M.; Lee, J. K.; Dabbousi, B. O.; Mikulec, F. V.; Bawendi, M. G. *J. Chem. Phys.* **1997**, *106*, 9869–9882.
(28) Ridley, B. A.; Nivi, B.; Jacobson, J. M. *Science* **1999**, *286*, 746–749.
(29) Purkayastha, A.; Kim, S.; Gandhi, D. D.; Ganesan, P. G.; Borca-Tasciuc, T.; Ramanath, G. *Adv. Mater.* **2006**, *18*, 2958–2963.
(30) Dirmyer, M. R.; Martin, J.; Nolas, G. S.; Sen, A.; Badding, J. V. *Small* **2009**, *5*, 933–937.
(31) Scheele, M.; Oeschler, N.; Meier, K.; Kornowski, A.; Klinke, C.; Weller, H. *Adv. Funct. Mater.* **2009**, *19*, 3476–3483.
(32) Wang, R. Y.; Feser, J. P.; Gu, X.; Yu, K. M.; Segalman, R. A.; Majumdar, A.; Milliron, D. J.; Urban, J. J. *Chem. Mater.* **2010**, *22*, 1943–1945.
(33) Kovalenko, M. V.; Scheele, M.; Talapin, D. V. *Science* **2009**, *324*, 1417–1420.
(34) Mitzi, D. B. *Adv. Mater.* **2009**, *21*, 3141–3158.

forming a dark brown solution after stirring for 10 days at room temperature. *Caution! Pure hydrazine is a toxic and flammable chemical and must be handled with care.* The resulting solution was filtered through a 0.2 μm PTFE filter to remove traces of undissolved material. Soluble Sb_2Se_3 precursor was prepared similarly to the procedure described by Milliron et al.[35] Sb_2Se_3 powder (480 mg, 1 mmol) and Se/N_2H_4 solution (2 mL, 0.5 M) were combined and formed a clear red solution after 2 days of stirring at room temperature.

Nanocrystal Synthesis. *PbTe NCs* were prepared by a slightly modified version of the procedure of Urban et al..[36] See details in the Supporting Information.[37] *PbS NCs* capped with oleic acid were synthesized according to the procedure developed by Hines et al.[38] The synthesis of *Bi_2S_3 NCs* is described in the Supporting Information.

Preparation of PbTe NCs Capped with Sb_2Te_3-MCCs. A two-phase mixture was prepared inside a glovebox by combining purified PbTe NCs in toluene (0.5 mL, 0.05 M referring to Pb), hexane (6 mL), Sb_2Te_3-MCCs (0.3 mL, 0.04 M referring to Sb), and hydrazine (4 mL). The obtained solution was stirred for no longer than 10−20 min, until the hexane phase became colorless, indicating the completion of the ligand exchange process. The upper organic phase was discarded and the hydrazine solution was washed three times with anhydrous hexane and filtered through a 0.2 μm PTFE filter. A purified hydrazine solution of PbTe NCs functionalized with Sb_2Te_3-MCCs was mixed with acetonitrile in a 2:1 volume ratio, which induced the flocculation of PbTe NCs. After centrifuging, the supernatant containing excessive Sb_2Te_3-MCCs not bound to the NC surface was discarded and the NCs were redispersed in 1 mL of hydrazine, forming a stable colloidal solution.

Preparation of Bi_2S_3 NCs Functionalized with Sb_2Te_3-MCCs. A solution of Bi_2S_3 nanorods in toluene (0.5 mL, 0.032 M referring to Bi_2S_3 formula unit) and hexane (8 mL) were combined with Sb_2Te_3-MCCs in N_2H_4 (0.3 mL, 0.08 M referring to Sb) and an additional 2.5 mL of N_2H_4. The solution was vigorously stirred for 5−15 min, until the transfer of nanorods into the N_2H_4 phase was completed. The organic phase was discarded, while the N_2H_4 phase was rinsed three times with anhydrous hexane and filtered through a 0.45 μm PTFE filter. Only freshly prepared solutions were used for the fabrication of $(Bi,Sb)_2Te_3$ thin films. The Bi:Sb molar ratio can be adjusted by tuning the ratio of Bi_2S_3 nanorods to Sb_2Te_3-MCCs, while providing a sufficient amount of Te to replace S. If necessary, additional Te can be added in the form of a solution of elemental Te in N_2H_4. In this study, all samples contained 60 ± 10% of Bi_2Te_3. To prepare Se-doped material, 10 mol % of Sb_2Se_3 was added to the above solution.

Preparation of PbS NCs/Sb_2Te_3-MCCs Solution. This was prepared analogously to the above example of Bi_2S_3 nanorods. PbS NCs in toluene (0.2 mL, 0.33 M referring to Pb) and hexane (4 mL) were combined with Sb_2Te_3-MCCs in hydrazine (0.38 mL, 0.06 M referring to Sb) and hydrazine (2.5 mL), followed by the same washing procedure.

Fabrication of Thin Film Devices. The above-described NC-MCC solutions will hereafter be referred to as "NC-inks". All samples for electrical conductivity and thermopower measurements were fabricated on glass substrates. Ti/Au contacts were either prepatterned on the substrate prior to deposition (bottom contacts) or were thermally evaporated after the film formation (top contacts, no Ti adhesion layer). In both cases the same channel length of 3 mm and width of 5 mm were maintained. Substrates were freshly hydrophilized by 15 min treatment with oxygen plasma. The NC-ink was then deposited by drop casting at 80 °C or by spray coating. The homogeneity and thickness of the drop-cast films were adjusted by controlling the volume and the concentration of NC-ink. 1−10% v/v DMSO was usually added to N_2H_4 solutions to improve the homogeneity of drop-cast films. For spray coating, glass substrates were placed on a hot plate at 100−200 °C, while a $(Bi,Sb)_2Te_3$ NC-ink solution was applied at a sprayer pressure of 15−20 psi using N_2 as a carrier gas. The film thickness was adjusted by the number of applied spraying cycles, typically 5−80. As-deposited $(Bi,Sb)_2Te_3$ films were heated at 300 °C/h and annealed at 300 °C for 15 min, followed by slow cooling to room temperature.

Structural and Optical Characterization. Experimental details related to the structural and optical characterization are provided in the Supporting Information.

Electrical Conductivity and Thermopower Measurements. The conductivity of NC films was measured using conventional two- and four-probe configurations and gold as the electrode material. The accurate thickness and roughness of the samples used for electrical measurements were obtained by atomic force microscopy (AFM), using a Veeco Nanoscope IIIa scanning probe microscope (Digital Instruments), as illustrated in Figure S1.[37]

The thermopower measurements were carried out in the 295−523 K temperature range using the homemade setup shown in Figure S2.[37] In order to determine the Seebeck coefficient, a temperature gradient (ΔT) of 0−20 K was applied across the sample by two platinum heating elements (Case Western University Electronic Design), powered by a Keithley 2400 source meter. The temperature gradient was measured by two resistive temperature detectors (RTDs, Omega) on an identical substrate symmetrically positioned close to the actual sample. A Keithley 2400 source meter and an Agilent 34410A multimeter operated by LabView were used for data acquisition. The open circuit voltage V_{OC} was measured as a function of ΔT, while the Seebeck coefficient was estimated as $S = -dV_{OC}/dT$, meaning that the higher potential at the cold side corresponds to a positive Seebeck coefficient (i.e., p-type material).

Thermal Conductivity Measurements. The thermal conductivity (κ) was measured in a temperature range from 298 to 575 K using the flash diffusivity method (LFA 457 laser flash apparatus, Netzsch Instruments, Inc.). NC-inks identical with those used for thin film deposition were pressed in form of disk-shaped samples (8 mm diameter; ∼0.6 mm thickness). The front face of the samples was irradiated by a short laser pulse, and the resulting rear face temperature rise was recorded and analyzed. Thermal conductivity (κ) values were calculated as $\kappa = \alpha C_p d$, where α is the thermal diffusivity, C_p is the specific heat measured from the differential scanning calorimetry, and d is the bulk density of the sample.

3. Results and Discussion

The synthesis of nanostructured TE materials, outlined in Figure 1, started with the exchange of the organic coating of as-synthesized colloidal NCs (Bi_2S_3, PbS, PbTe, Figure 1A) with Sb_2Te_3-MCCs. The resulting all-inorganic "NC-ink" was used for solution deposition of solid materials by drop casting, spray coating, or drying/hot pressing (Figure 1B).

Preparation of Sb_2Te_3-MCC and Sb_2Se_3-MCC in Hydrazine. We prepared a soluble molecular precursor for the crystalline Sb_2Te_3 phase by adopting the methodology pioneered by Mitzi.[41,42] Various metal chalcogenide complexes can be formed by dissolving bulk metal chalcogenides in N_2H_4 in the presence of elemental chalcogens. The soluble species usually contain chalcogenidometalate anions charge-balanced by hydrazinium

(35) Milliron, D. J.; Raoux, S.; Shelby, R.; Jordan-Sweet, J. *Nat. Mater.* **2007**, *6*, 352–356.
(36) Urban, J. J.; Talapin, D. V.; Shevchenko, E. V.; Murray, C. B. *J. Am. Chem. Soc.* **2006**, *128*, 3248–3255.
(37) For more details see the Supporting Information.
(38) Hines, M. A.; Scholes, G. D. *Adv. Mater.* **2003**, *15*, 1844–1849.
(39) Rietveld, H. M. *J. Appl. Crystallogr.* **1969**, *2*, 65–71.
(40) McCusker, L. B.; Von Dreele, R. B.; Cox, D. E.; Louer, D.; Scardi, P. *J. Appl. Crystallogr.* **1999**, *32*, 36–50.
(41) David, B. M. *Adv. Mater.* **2009**, Early View.
(42) Mitzi, D. B.; Kosbar, L. L.; Murray, C. E.; Copel, M.; Afzali, A. *Nature* **2004**, *428*, 299–303.

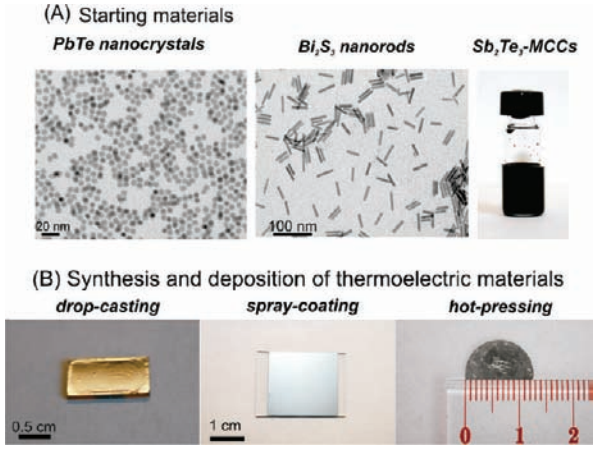

Figure 1. Preparation of nanostructured thermoelectric $(Bi,Sb)_2Te_3$ and PbTe-Sb_2Te_3 materials: (A) PbTe NCs and Bi_2S_3 nanorods capped with the organic ligands and a solution of Sb_2Te_3-MCCs (molecular metal chalcogenide complex) used as starting materials; (B) colloidal solution of NCs functionalized with Sb_2Te_3-MCCs used in various ways to synthesize and deposit a thermoelectric material (from left to right: drop-cast thin film of PbTe NCs capped with Sb_2Te_3-MCCs, spray-coated $(Bi,Sb)_2Te_3$ thin film, and a $(Bi,Sb)_2Te_3$ pellet).

$N_2H_5^+$ cations and additional N_2H_4 molecules incorporated via hydrogen bonding. This enables a vast diversity of structures, including discrete Zintl ions such as $Sn_2S_6^{4-}$ and $Sn_2Se_6^{4-}$,[42] layered $N_4H_9Cu_7S_4$ complexes,[43] one-dimensional covalent $(N_2H_4)_2ZnTe$,[44] and mixed metallic $[Mn_2SnE_4(N_2H_4)_n]$ (E = S, Se; $n = 2-5$) species.[45,46] The ability of these complexes to form pure parent metal chalcogenides upon mild heat treatment (100−350 °C) is currently being studied for the solution-based deposition of technologically relevant metal chalcogenides such as photovoltaic $CuIn_xGa_{1-x}Se_2$,[47,48] phase-change KSb_5S_8[49] and GeSbSe,[35] and high-mobility semiconducting n-$SnS_{2-x}Se_x$,[42] n-In_2Se_3,[50] and p-$CuInTe_2$[51] thin films.

Dark brown Sb_2Te_3-MCC (Figure 1A) and light red Sb_2Se_3-MCC solutions were prepared by the room-temperature dissolution of bulk Sb_2Te_3 and Sb_2Se_3 in N_2H_4 in the presence of additional elemental Te and Se, respectively. Red crystals of $(N_2H_4)(N_2H_5)_3SbSe_4$[52] were isolated from Sb_2Se_3-MCC solution, and their molecular structure was confirmed by X-ray diffraction. Sb_2Te_3-MCC could not be crystallized using similar approaches because of its instability: Sb_2Te_3-MCC decomposed into rhombohedral Sb_2Te_3 and elemental Te upon solvent evaporation, as confirmed by the powder XRD studies in Figure S3.[37] TGA scans of the solid residue obtained by drying Sb_2Te_3-MCC at room temperature revealed weight loss of only ~1% upon heating to 350 °C in Figure S4,[37] pointing to the complete decomposition of Sb_2Te_3-MCC. The major weight loss occurred at temperatures above 450 °C, due to the evaporation of elemental tellurium.

We applied a suite of characterization techniques providing information about the nature of species present in Sb_2Te_3-MCC solutions. ICP-OES elemental analysis showed that Sb_2Te_3 completely dissolved in N_2H_4 only for the overall Te/Sb ratios of ≥3.5, pointing to the fact that additional Te is needed to coordinate Sb. There are only few relevant examples in the literature, such as $Sb_2Te_5^{4-}$ Zintl anions formed by cathodic dissolution of Sb_2Te_3[53,54] and melt-synthesized K_3SbTe_3,[55] supporting the formation of the small discrete Sb−Te species, seen in our case. To provide a direct insight into the composition of soluble Sb_2Te_3-MCC species, we carried out electrospray ionization mass spectrometry (ESI-MS) analysis of Sb_2Te_3-MCC in N_2H_4 in Figure S5.[37] Detected soluble antimony telluride complexes showed Sb nuclearity of one or two, such as $SbTe_3^{3-}$, $Sb_2Te_5^{4-}$, and $Sb_2Te_7^{4-}$ and no heavier moieties. In agreement with ESI-MS, dynamic light scattering (DLS) measurements, with sensitivity down to ≤1 nm,[56] did not reveal the presence of any large, e.g., oligomeric, polymeric, or colloidal, species. To summarize, ESI-MS measurements suggest that Sb_2Te_3-MCC solutions contain $SbTe_3^{3-}$, $Sb_2Te_5^{4-}$, and $Sb_2Te_7^{4-}$ Zintl ions as the dominant species. The elemental analysis agrees best with the $Sb_2Te_7^{4-}$ composition, which has not been previously reported and is probably structurally similar to $Sb_2Te_5^{4-}$ species with two Te^{2-} atoms substituted for $(Te_2)^{2-}$ groups. At the same time, we cannot exclude the coexistence of several species in Sb_2Te_3-MCC solutions in chemical equilibrium with each other.

PbTe NCs Functionalized with Sb_2Te_3-MCCs. PbTe is one of the most efficient TE materials, with optimal *ZT* values between 300 and 600 °C,[4,57] and is currently used in high-temperature power generation modules.[8] At the same time, PbTe has a large Bohr excitonic radius of 46 nm,[58] which makes it an especially convenient material for achieving strong electronic quantum confinement, potentially beneficial for studying the effect of size quantization on the Seebeck coefficient. A large static dielectric constant ($\varepsilon \approx 1000$)[59] reduces the Coulomb charging energy, facilitating charge transport through granular films and NC solids.

PbTe NCs in the 2−30 nm size range were synthesized in organic solvents using a well-established hot-injection method.[36,60] The original oleic acid capping molecules were replaced by Sb_2Te_3-MCCs in a simple phase-transfer procedure, by combining PbTe NCs in hexane with Sb_2Te_3-MCCs in N_2H_4. Upon vigorous stirring, the original organic ligands remained in the hexane phase, while PbTe NCs turned hydrophilic and became highly soluble in hydrazine and its mixtures with common polar solvents such as DMSO and formamide. The mean size and monodispersity of the NCs (Figure 2A) were retained in the course of ligand exchange, as was evidenced by comparing with original NCs in Figure S6.[37] Furthermore, no changes in either

(43) Mitzi, D. B. *Inorg. Chem.* **2007**, *46*, 926–931.
(44) Mitzi, D. B. *Inorg. Chem.* **2005**, *44*, 7078–7086.
(45) Manos, M. J.; Kanatzidis, M. G. *Inorg. Chem.* **2009**, *48*, 4658–4660.
(46) Yuan, M.; Dirmyer, M.; Badding, J.; Sen, A.; Dahlberg, M.; Schiffer, P. *Inorg. Chem.* **2007**, *46*, 7238–7240.
(47) Mitzi, D. B.; Yuan, M.; Liu, W.; Kellock, A. J.; Chey, S. J.; Gignac, L.; Schrott, A. G. *Thin Solid Films* **2009**, *517*, 2158–2162.
(48) Mitzi, D. B.; Yuan, M.; Liu, W.; Kellock, A. J.; Chey, S. J.; Deline, V.; Schrott, A. G. *Adv. Mater.* **2008**, *20*, 3657–3660.
(49) Mitzi, D. B.; Raoux, S.; Schrott, A. G.; Copel, M.; Kellock, A.; Jordan-Sweet, J. *Chem. Mater.* **2006**, *18*, 6278–6282.
(50) Mitzi, D. B.; Copel, M.; Chey, S. J. *Adv. Mater.* **2005**, *17*, 1285–1289.
(51) Mitzi, D. B.; Copel, M.; Murray, C. E. *Adv. Mater.* **2006**, *18*, 2448–2452.
(52) Mitzi, D. B. Private communication.
(53) Warren, C. J.; Dhingra, S. S.; Ho, D. M.; Haushalter, R. C.; Bocarsly, A. B. *Inorg. Chem.* **1994**, *33*, 2709–2710.
(54) Warren, C. J.; Haushalter, R. C.; Bocarsly, A. B. *J. Alloys Compd.* **1995**, *229*, 175–205.
(55) Jung, J. S.; Wu, B. O.; Stevens, E. D.; Oconnor, C. J. *J. Solid State Chem.* **1991**, *94*, 362–367.
(56) Kaszuba, M.; McKnight, D.; Connah, M. T.; McNeil-Watson, F. K.; Nobbmann, U. *J. Nanopart. Res.* **2008**, *10*, 823–829.
(57) Dughaish, Z. H. *Phys. B* **2002**, *322*, 205–223.
(58) Wise, F. W. *Acc. Chem. Res.* **2000**, *33*, 773–780.
(59) *Landolt-Bornstein*; Springer-Verlag: Berlin, 1983; Vol. 17.
(60) Murphy, J. E.; Beard, M. C.; Norman, A. G.; Ahrenkiel, S. P.; Johnson, J. C.; Yu, P. R.; Micic, O. I.; Ellingson, R. J.; Nozik, A. J. *J. Am. Chem. Soc.* **2006**, *128*, 3241–3247.

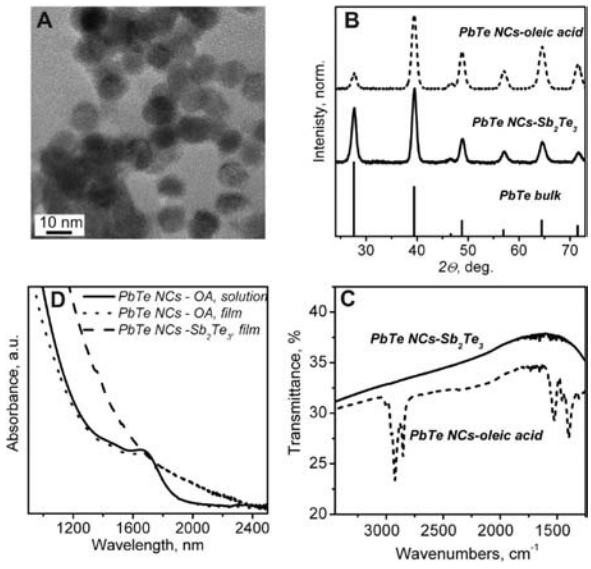

Figure 2. (A) TEM image of PbTe NCs capped with Sb_2Te_3-MCCs. (B−D) Comparative study of PbTe NC solids capped with original oleic acid ligands and with Sb_2Te_3-MCCs using (B) powder XRD, (C) FTIR spectroscopy, and (D) near-IR optical absorption spectroscopy.

the crystal structure or in the mean crystallite size were detected by powder XRD studies (Figure 2B). The completeness of the ligand exchange was confirmed by comparing the FTIR spectra for NC solids before and after the phase-transfer procedure (Figure 2C), where the latter samples showed the complete disappearance of C−H stretching and bending modes. We also found that XRD patterns for both the as-deposited (80 °C) and annealed (300 °C) samples showed reflections from the only PbTe phase in Figure S7A,[37] excluding the formation of extended domains of Sb_2Te_3 or Te phases in the samples purified from excessive Sb_2Te_3 MCCs. The Scherrer size of PbTe grains increased from ∼10 nm to ∼30 nm upon annealing at 300 °C, pointing to partial sintering of PbTe NCs. Furthermore, TGA scans revealed a very small weight loss (2−3%) during sample annealing in Figure S4.[37]

The solubility of MCC-functionalized NCs in hydrazine and other common polar solvents enables the facile solution deposition of macroscopically homogeneous NC films (Figure 1B) with typical thicknesses of 0.1−0.4 μm and root-mean-square (rms) roughness of 10−20 nm. Such films could be deposited on highly hydrophilic substrate surfaces, given that NC concentration and drying temperature were optimized. As compared to the hydrazine chemical activation of organics-capped PbTe and PbSe NC solids,[36,61−63] our new approach is not limited to thin films, does not cause cracking of the films due to the shrinking of NCs, and ensures the complete removal of organic molecules.

The absorption spectra for the films of oleic-acid capped PbTe NCs closely resembled spectra for the colloidal solution with a well-resolved $1S_h-1S_e$ optical transition, indicating the strong localization of excitons on individual quantum dots (Figure 2D). In contrast, the spectrum of PbTe NCs capped with Sb_2Te_3-MCCs appears featureless with an absorption tail extending further in the infrared. The absorption tail could originate from surface-bound Sb_2Te_3-MCCs. At the same time, the red shift points to partial relaxation of the quantum confinement due to strong electronic coupling between MCC-capped NCs.

As-deposited films of PbTe NCs capped with Sb_2Te_3-MCCs exhibited ohmic $I-V$ characteristics with conductivities of ∼0.05 S cm^{-1}, which corresponds to an ∼10 orders of magnitude increase compared to that of oleic-acid capped PbTe NCs ($\sigma \approx 10^{-12}$ S cm^{-1}). The low-temperature (4−300 K) dependence of conductance (G) followed non-Arrhenius behavior, $G \approx \exp(1/T^n)$ with $n = 1/4$ (Figure S8A (Supporting Information)). $n = 1/4$ is characteristic of the three-dimensional Mott-type variable-range hopping, in which the hopping electrons find the optimal path with the lowest activation energy and the shortest hopping distance, while the Coulomb interactions are small due to the large dielectric constants of both PbTe and Sb_2Te_3.[64] For these samples we also found very high values of the Seebeck coefficient up to +750 μV/K in Figure S8B.[37] From field-effect transistor measurements we determined the hole mobility $\mu \approx 0.24$ cm^2 V^{-1} s^{-1} and the majority carrier (hole) density $n \approx 1.3 \times 10^{18}$ cm^{-3} in Figure S8C and S9.[37] For comparable carrier density, our PbTe NCs solids show a more than 2-fold increase in thermopower in comparison to bulk PbTe.[12] As a plausible explanation, quantum confinement leads to sharp spikes in the density of electronic states (DOS) of PbTe NCs as compared to the parabolic DOS in bulk semiconductors.[65] Chemically synthesized PbTe nanowires with diameters of 10−40 nm were recently reported to exhibit enhanced Seebeck coefficients of 410−628 μV/K.[66,67] In a single report of TE properties for colloidally synthesized PbTe NCs,[68] for samples prepared by sintering relatively large (30−50 nm) and irregularly shaped particles, an enhanced Seebeck coefficient of above 500 μV/K has been shown. In agreement with current findings, our previous studies revealed enhanced and size-dependent Seebeck coefficients of 700−1150 μV/K in the arrays of hydrazine-treated PbSe NCs.[65]

Unlike in previous reports for organics-capped PbTe NCs,[36,63] the hydrazine treatment of MCC-capped PbTe NCs neither changed the type of majority carriers nor notably affected the film conductivity. We then concluded that stable p-type conductivity was determined by excess Te from surface-bound Sb_2Te_3-MCCs. A slight excess of Te is a typical method for the p-type doping of PbTe.[8]

The annealing of MCC-capped PbTe NCs at 300 °C increases conductivity up to 19 S cm^{-1} due to the partial sintering of PbTe NCs, as confirmed by powder XRD in Figure S7A[37] and TEM in Figure S7B.[37] In order to make TE material practical for high-temperature operation, it will be necessary to develop some means of control over the average grain size. Currently we are studying the effect of Sb_2Te_3 content and temperature history on the granularity and TE characteristics of this material. As an alternative approach to address these problems in the same materials system, we explored the in situ conversion of PbS NCs into PbTe.

(61) Talapin, D. V.; Murray, C. B. *Science* **2005**, *310*, 86–89.
(62) Law, M.; Luther, J. M.; Song, Q.; Hughes, B. K.; Perkins, C. L.; Nozik, A. J. *J. Am. Chem. Soc.* **2008**, *130*, 5974–5985.
(63) Urban, J. J.; Talapin, D. V.; Shevchenko, E. V.; Kagan, C. R.; Murray, C. B. *Nat. Mater.* **2007**, *6*, 115–121.
(64) Yu, D.; Wang, C. J.; Wehrenberg, B. L.; Guyot-Sionnest, P. *Phys. Rev. Lett.* **2004**, *92*, 216802.
(65) Wang, R. Y.; Feser, J. P.; Lee, J.-S.; Talapin, D. V.; Segalman, R.; Majumdar, A. *Nano Lett.* **2008**, *8*, 2283–2288.
(66) Tai, G.; Zhou, B.; Guo, W. L. *J. Phys. Chem. C* **2008**, *112*, 11314–11318.
(67) Yan, Q. Y.; Cheng, H.; Zhou, W. W.; Hug, H. H.; Yin, F.; Boey, C.; Ma, J. *Chem. Mater.* **2008**, *20*, 7364–7364.
(68) Zhou, W. W.; Zhu, J. X.; Li, D.; Hng, H. H.; Boey, F. Y. C.; Ma, J.; Zhang, H.; Yan, Q. Y. *Adv. Mater.* **2009**, *21*, 3196–3200.

PbTe-Sb_2Te_3 Nanocomposites through in Situ Conversion of PbS NCs to PbTe. In the previous example small amounts ($\leq$20%) of Sb_2Te_3-MCCs were used as a conductive capping material, acting as an "electronic glue", for improved charge transport in NC solids. At the same time, many practical TE materials contain significantly larger contents of Sb_2Te_3.[3,8] Due to the large excess of Te, an Sb_2Te_3-MCC precursor may be impractical for generating a stoichiometric Sb_2Te_3 phase without the high-temperature anneals necessary to evaporate excess Te. Here, we discuss an approach in which excessive Te is purposefully used to make complex telluride TE materials.

We fabricated n-type PbTe-Sb_2Te_3 nanocomposite materials using colloidally synthesized PbS NCs and Sb_2Te_3-MCCs. The solution of PbS NCs functionalized with Sb_2Te_3-MCCs was prepared analogously to the previous PbTe NCs/Sb_2Te_3-MCCs system using the ligand-exchange procedure, except for one key difference—excess Sb_2Te_3-MCC was not removed after the ligands exchange. The excess MCC was used in subsequent chemical transformations as a source of elemental Te. Upon raising the temperature to 300 °C, we observed the transformation of PbS NCs into the PbTe phase, which was driven by the dynamic shift of equilibrium due to the evaporation of sulfur (PbS + Te = PbTe + S$\uparrow$). PbTe and Sb_2Te_3 phases are largely immiscible.[69,70] Both phases are clearly seen in powder XRD patterns for samples annealed at 300 °C in Figure S10.[37] In fact, the immiscibility of PbTe and Sb_2Te_3 was recently utilized by Snyder et al.[71,72] for the formation of nanometer lamellae of PbTe and Sb_2Te_3 with epitaxy-like interfaces by means of rapid solidification from melts.

Our preliminary TE characterizations showed rather high electrical conductivities of 80−160 S cm^{-1}, depending upon the film uniformity, which is far higher than conductivities for PbTe NCs capped with Sb_2Te_3-MCCs. The Seebeck coefficient of -90 ± 10 μV/K points to n-type conductivity, in agreement with $S = -50 \pm 10$ μV/K reported by Shyder et al. for melt-solidified PbTe/Sb_2Te_3.[71,72] The biphase PbTe/Sb_2Te_3 composite exhibited an increase in electrical conductivity with increasing temperature in Figure S11[37] and remarkably low temperature dependence of *S*, which can be related to the peculiar chemical and crystal structure of this material. The availability of large-scale synthetic methods for colloidal PbS NCs[38,73] is a very practical advantage of this approach.

Nanostructured $(Bi,Sb)_2Te_3$ Alloys through Nanoscale Solid-State Chemical Transformations. Alloying of Bi_2Te_3 with Sb_2Te_3 is a standard method for decreasing thermal conductivity by introducing disorder in the unit cell, while the electrical conductivity remains high.[4,8] Our attempts to prepare a soluble molecular precursor for $(Bi,Sb)_2Te_3$ by combining Sb_2Te_3-MCC and Bi_2Te_3-MCC failed because Bi(III) chalcogenides could not form stable molecular precursors in hydrazine in the presence of elemental S, Se, or Te. Furthermore, to enhance the TE performance by nanostructuring, we need some means of controlling the grain size in $(Bi,Sb)_2Te_3$. To address these issues, we have developed an approach in which a Bi chalcogenide phase was introduced in the form of Bi_2S_3 NCs (Figure 1A). The synthesis of colloidal Bi_2S_3 nanostructures has been previously reported by several groups.[74−76] In this study we used a simple method utilizing Bi(III) acetate and elemental sulfur as precursors, oleic acid as capping ligand, and octadecene as a solvent. By varying the concentration of reagents, nearly spherical in Figure S12[37] and rod-shaped (Figure 1A) Bi_2S_3 NCs were synthesized. The longitudinal axis of the nanorods was the (002) direction, confirmed by the powder XRD studies (Figure 3a). In the following, all results were obtained and demonstrated using rod-shaped Bi_2S_3 NCs.

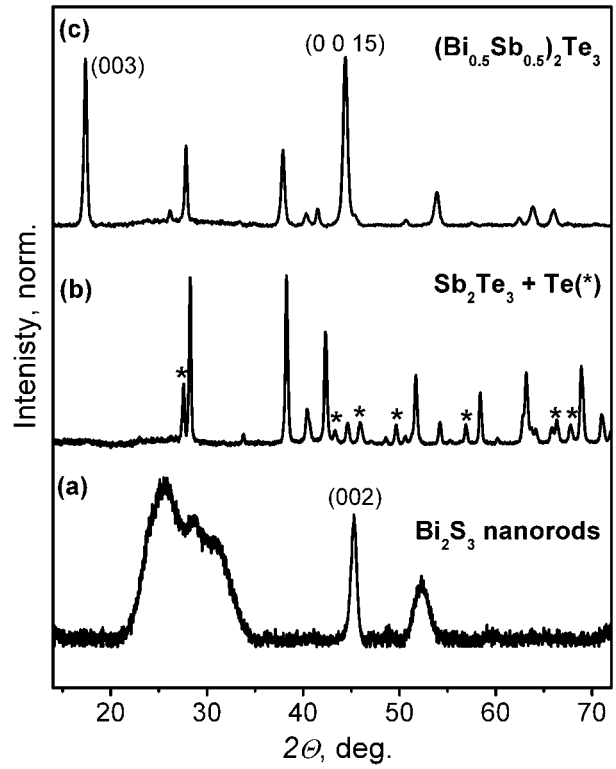

Figure 3. Formation of $(Bi_{0.5}Sb_{0.5})_2Te_3$ nanocomposite through solid-state reactions between Bi_2S_3 nanorods and Sb_2Te_3-MCCs: X-ray diffraction patterns of (a) oleic-acid capped Bi_2S_3 nanorods, (b) Sb_2Te_3-MCCs, dried and annealed at 300 °C, and (c) pure phase $(Bi_{0.5}Sb_{0.5})_2Te_3$ alloy film, annealed at 300 °C. No traces of excessive Te could be detected in $(Bi_{0.5}Sb_{0.5})_2Te_3$ for the correctly adjusted molar ratio Bi_2S_3/Te/Sb_2Te_3. All peaks were assigned and referenced to the PDF-2 file (ICDD) for Bi_2S_3 (17-0320, Bismuthinite, orthorhombic), Sb_2Te_3 (15-0874, rhombohedral), Te (72-6647, hexagonal) and $(Bi_{0.5}Sb_{0.5})_2Te_3$ (72-1835, rhombohedral). An enlarged XRD pattern of $(Bi_{0.5}Sb_{0.5})_2Te_3$ along with bulk reflections from the PDF-2 database are shown in Figure S13 (Supporting Information).

The solution of Bi_2S_3 rods capped with Sb_2Te_3-MCCs was prepared following the ligand-exchange procedure, with an adjustable amount of excess Sb_2Te_3-MCCs. The formation of $(Bi,Sb)_2Te_3$ phase occurs as follows:

(69) Wood, C. *Rep. Prog. Phys.* **1988**, 459–539.
(70) Abrikosov, N. K.; Elagina, E. I.; Popova, M. A. *Inorg. Mater.* **1965**, *1*, 1944–1946.
(71) Ikeda, T.; Collins, L. A.; Ravi, V. A.; Gascoin, F. S.; Haile, S. M.; Snyder, G. J. *Chem. Mater.* **2007**, *19*, 763–767.
(72) Ikeda, T.; Ravi, V. A.; Snyder, G. J. *Acta Mater.* **2009**, *57*, 666–672.
(73) Cademartiri, L.; Bertolotti, J.; Sapienza, R.; Wiersma, D. S.; von Freymann, G.; Ozin, J. *J. Phys. Chem. B* **2006**, *110*, 671–673.
(74) Malakooti, R.; Cademartiri, L.; Akcakir, Y.; Petrov, S.; Migliori, A.; Ozin, G. A. *Adv. Mater.* **2006**, *18*, 2189–2194.
(75) Cademartiri, L.; Malakooti, R.; O'Brien, P. G.; Migliori, A.; Petrov, S.; Kherani, N. P.; Ozin, G. A. *Angew. Chem., Int. Ed.* **2008**, *47*, 3814–3817.
(76) Sigman, M. B.; Korgel, B. A. *Chem. Mater.* **2005**, *17*, 1655–1660.

$$Sb_2Te_3\text{-MCC} \rightarrow Sb_2Te_3 + Te + N_2H_4 \quad (1)$$

$$Bi_2S_3 \text{ nanorods} + 3Te \rightarrow Bi_2Te_3 + 3S\uparrow \quad (2)$$

$$xSb_2Te_3 + (2-x)Bi_2Te_3 \rightarrow 2Bi_{2-x}Sb_xTe_3 \quad (3)$$

All three reactions occur during the annealing of the composite films. Decomposition of the molecular precursor (reaction 1) takes place as soon as the film is dried. Released Te replaces sulfur in Bi_2S_3 (reaction 2). This replacement is facilitated by the evaporation of elemental sulfur. In fact, the S^{2-}-to-Te^{2-} anion exchange may slowly occur even in solution. Alloying (reaction 3) requires higher temperatures and occurs only upon annealing at 180 °C or above.

The small size of the NCs offers unique possibilities for these solid-state chemical transformations. The size of the NCs is comparable to the best available estimates for the width of the reaction zone in solid-state reactions.[77] This correlates with the fast and complete reactions of NCs, such as cation exchange,[78,79] oxidation and sulfuration,[80] carried out in colloidal solutions. The present study demonstrates the possibility to perform solid-state material synthesis using chemical transformations of colloidal NCs to form a phase-pure material by anion exchange and alloying.

An easy track of reactions 1−3 is provided by powder XRD patterns (Figure 3). The original Bi_2S_3 nanorods show the diffraction peaks with significant Scherrer broadening (Figure 3a). Reaction 1 provides a required amount of crystalline Te and Sb_2Te_3 (Figure 3b) needed for the formation of phase-pure $(Bi_{0.5}Sb_{0.5})_2Te_3$ upon the film annealing at 300 °C in Figure 3c and Figure S13.[37] Note that the XRD reflections from $(Bi_{0.5}Sb_{0.5})_2Te_3$ are usually considerably broader than the Sb_2Te_3 reflections observed in the absence of Bi_2S_3 nanorods, which we attribute to the effect of NC size on the grain size in the final TE material. The angular position of the diffraction peaks of the $(Bi_{0.5}Sb_{0.5})_2Te_3$ phase closely match the rhombohedral $(Bi_{0.5}Sb_{0.5})_2Te_3$ phase from the PDF-2 database (72-1835). A preferential crystallographic orientation in thin films of $(Bi_{0.5}Sb_{0.5})_2Te_3$ is another general observation, which is evidenced from the enhancement of the (001)-relevant reflections, whose intensity is generally low for a powdered bulk material. Rietveld refinement, exemplarily shown in Figure S14,[37] confirmed the formation of a pure $(Bi_{0.5}Sb_{0.5})_2Te_3$ phase with an average domain size of 30−50 nm.

A careful adjustment of reagent quantities is necessary to obtain single-phase material. For example, if the amount of Bi_2S_3 nanorods is not sufficient to convert all Te, additional peaks appear in XRD patterns at 2θ angles of 27.7, 43.5, and 57.0° corresponding to the hexagonal Te phase in Figure S15A.[37] In an opposite case, when a large excess of Bi_2S_3 nanorods is used, the final material contains a tetradymite Bi_2Te_2S phase in Figure S15B,[37] a highly stable material with rhombohedral crystal structure. Sulfur is a known n-type dopant for Bi_2Te_3.[81] The formation of an undesired Bi_2Te_2S phase[29] or contamination by sulfur[30] was found in the nanostructures formed by sintering thiol-capped Bi_2Te_3 NCs, which caused the material to be n-type

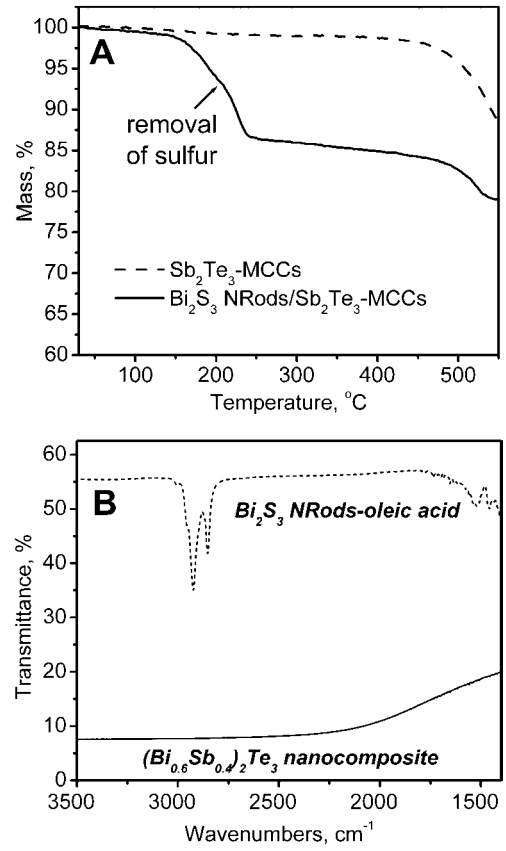

Figure 4. (A) TGA scans for Bi_2S_3/Sb_2Te_3-MCCs dried samples showing the release of S in the course of solid-state chemical transformation toward the $(Bi_{0.6}Sb_{0.4})_2Te_3$ phase. (B) FTIR spectra for oleic-acid capped Bi_2S_3 nanorods (dash line) and for a $(Bi_{0.6}Sb_{0.4})_2Te_3$ sample dried at 180 °C on a CaF_2 substrate.

conductive.[30] The observation of p-type conductivity for our $(Bi,Sb)_2Te_3$ samples provided an additional indirect confirmation of the efficient removal of sulfur during the anion exchange. The alloying of Bi_2Te_3 and Sb_2Te_3 (reaction 3) was evidenced from the gradual shift of XRD peaks to larger 2θ angles with an increase in Sb content. The shift is due to larger dimensions of the Bi_2Te_3 unit cell ($a = 4.386$ Å, $c = 30.497$ Å) compared to that of Sb_2Te_3 ($a = 4.264$ Å, $c = 30.458$ Å). The fractional occupancies of Bi and Sb were determined from Rietveld analysis in Figure S14[37] and are in good agreement with the initial molar ratios of Bi_2S_3 rods and Sb_2Te_3-MCCs.

TGA studies revealed that removal of S occurred in the temperature range of 150−220 °C (Figure 4A). This finding is consistent with XRD data, where $(Bi,Sb)_2Te_3$ peaks are observable only after annealing above 180 °C. FTIR spectra of samples dried at 180 °C showed the complete absence of the absorption features at 2800−3000 cm^{-1} corresponding to C−H stretching modes, indicative of the quantitative removal of the organic ligands (Figure 4B). As expected, the formation of a narrow-gap semiconductor phase increased absorption in the near- and mid-infrared spectral regions. A further decrease of absorption for photon energies less than 0.25 eV (>5 μm) could be due to proximity of the fundamental absorption edge of $(Bi,Sb)_2Te_3$.

Solution Deposition and Characterization of Thin $(Bi,Sb)_2Te_3$ Films. Fresh NC-inks were used for solution deposition of uniform TE films. Spin casting can generate

(77) Backhaus-Ricoult, M. *Annu. Rev. Mater. Res.* **2003**, *33*, 55–90.
(78) Son, D. H.; Hughes, S. M.; Yin, Y. D.; Alivisatos, A. P. *Science* **2004**, *306*, 1009–1012.
(79) Kovalenko, M. V.; Talapin, D. V.; Loi, M. A.; Cordella, F.; Hesser, G.; Bodnarchuk, M. I.; Heiss, W. *Angew. Chem., Int. Ed.* **2008**, *47*, 3029–3033.
(80) Yin, Y. D.; Rioux, R. M.; Erdonmez, C. K.; Hughes, S.; Somorjai, G. A.; Alivisatos, A. P. *Science* **2004**, *304*, 711–714.
(81) Durst, T.; Goldsmid, H. J.; Harris, L. B. *Sol. Energ. Mater.* **1981**, *5*, 181–186.

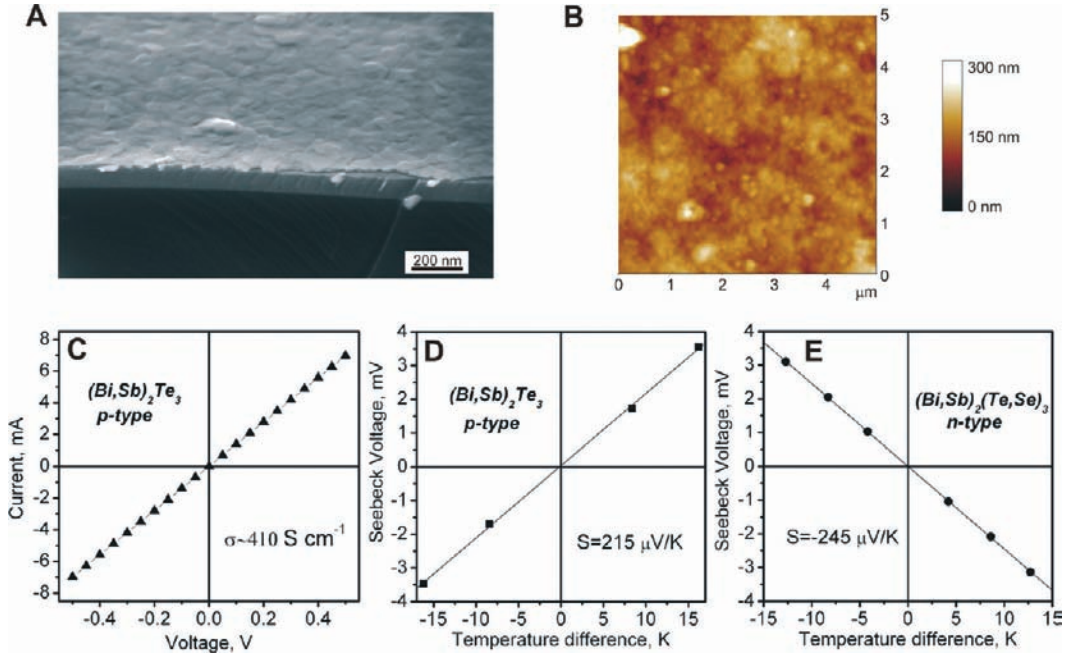

Figure 5. (A) Cross-sectional SEM image of a ~20 nm thick $(Bi_{0.5}Sb_{0.5})_2Te_3$ film prepared by spin casting. (B) Tapping-mode AFM image of 0.3 μm thick $(Bi_{0.5}Sb_{0.5})_2Te_3$ films prepared by drop casting. (C) $I-V$ curve and (D) a plot of Seebeck voltage vs temperature difference for a representative sample of a p-type $(Bi,Sb)_2Te_3$ spray-cast film. (E) Plot of Seebeck voltage vs temperature difference for an n-type $(Bi, Sb)_2(Te_{0.9}Se_{0.1})_3$ drop-cast film (~10 mol % of Sb_2Se_3).

smooth and continuous thin films (10−50 nm thick, Figure 5A); however, thicker films are required for practical TE applications. Therefore, further comparative studies were conducted on either drop-cast or spray-coated samples fabricated on glass substrates. Both techniques readily produce 0.1−0.4 μm thick films, with low surface roughness of 10−50 nm in Figure S5B and Figure S1.[37] Sample compositions were adjusted to $Bi_{1.2}Sb_{0.8}Te_3$ with ±10% batch-to-batch variations. All samples were annealed at 300 °C. $I-V$ curves for each sample with gold electrodes showed high conductivity and excellent linearity over the entire range of applied voltages. The measured conductivities for drop-cast films spread in a broad range from 30 to 200 S cm^{-1}, depending upon the concentration of cracks and other structural defects. In contrast, spray-coated samples on average showed higher conductivities of 200−450 S cm^{-1} at room temperature (Figure 5C). Thermopower measurements revealed p-type conductivity and Seebeck coefficients of ~170−250 μV/K (Figure 5D). Unlike electrical conductivity, which is very sensitive to homogeneity of the sample, thermopower is an inherent material property and is reproducible within ±10% for the series of same-formulated samples. Our values of S are similar to the previously reported value (~210 μV/K) for the bulk $(Bi,Sb)_2Te_3$ generated by hot-pressing ball-milled nanopowders,[18] which is currently the best bismuth−telluride material with conductivity in excess of 1000 S cm^{-1} and $ZT = 1.2$ at room temperature. Our solution-processed samples compare quite favorably with the vacuum-deposited thin film Bi−Te materials, which are naturally less conductive than bulk materials. Representative literature examples include flash-evaporated n-type Bi−Te-based thin films ($\sigma \approx 540$ S cm^{-1}),[82] flash-evaporated $Bi_{0.5}Sb_{1.5}Te_3$ thin films ($\sigma \approx 550$ S cm^{-1}),[83] coevaporated Bi_2Te_3 thin films ($\sigma \approx 166$,[22] 770 S cm^{-1} [23]), and sputtered Bi−Sb−Te thin films ($\sigma \approx 70-200$ S cm^{-1}).[84]

n-Type $(Bi,Sb)_2(Te,Se)_3$. Fabrication of TE modules requires both p- and n-type materials with similar TE properties. To control the type of majority carriers and doping level of our solution-derived materials, we used selenium as a convenient dopant for preparing n-type bismuth−antimony telluride.[85] Sb_2Se_3 (~10 mol %) was introduced into the ink in the form of Sb_2Se_3-MCCs in hydrazine, followed by the same ink preparation as before. The Seebeck coefficient of the resulting film is −245 μV/K, indicating n-type conductivity (Figure 5E). The conductivity of drop-cast Se-doped samples were found to be 100−200 S cm^{-1}, slightly lower than for p-type $(Bi,Sb)_2Te_3$.

The power factor $S^2\sigma$ of TE materials is usually strongly temperature-dependent due to the temperature dependencies of both S and σ. $S-T$ and $\sigma-T$ scans for p-type $(Bi,Sb)_2Te_3$ and n-type $(Bi,Sb)_2(Te,Se)_3$ are shown in Figure 6. For p-type $(Bi,Sb)_2Te_3$, σ decreased with temperature (Figure 6A), whereas S increased by 30 μV/K (Figure 6B) and the power factor $S^2\sigma$ was only about 20% smaller at 523 K (16.3 μW/cm K^2) in comparison to its room-temperature value (20.4 μW/cm K^2). For comparison, state-of-the-art p-type $(Bi,Sb)_2Te_3$ and recently reported high-performance "bulk" nanostructured $(Bi,Sb)_2Te_3$ lose correspondingly 78% and 55% of their $S^2\sigma$ in the same temperature range,[18] showing high-temperature power factors very similar to those of our samples.

Thermal Conductivity and ZT of Nanostructured $(Bi,Sb)_2Te_3$. To assess the heat transport properties of our solution-processed nanocomposites, we measured thermal conductivity using laser flash diffusivity technique. The measurements were carried out on the pellets (Figure 1B) prepared from the NC-inks followed by thermal annealing. Figure 7 shows

(82) Takashiri, M.; Takiishi, M.; Tanaka, S.; Miyazaki, K.; Tsukamoto, H. *J. Appl. Phys.* **2007**, *101*, 074301.
(83) Volklein, F.; Baier, V.; Dillner, U.; Kessler, E. *Thin Solid Films* **1990**, *187*, 253–262.
(84) Liao, C. N.; She, T. H. *Thin Solid Films* **2007**, *515*, 8059–8064.
(85) Ettenberg, M. H.; Maddux, J. R.; Taylor, P. J.; Jesser, W. A.; Rosi, F. D. *J. Cryst. Growth* **1997**, *179*, 495–502.

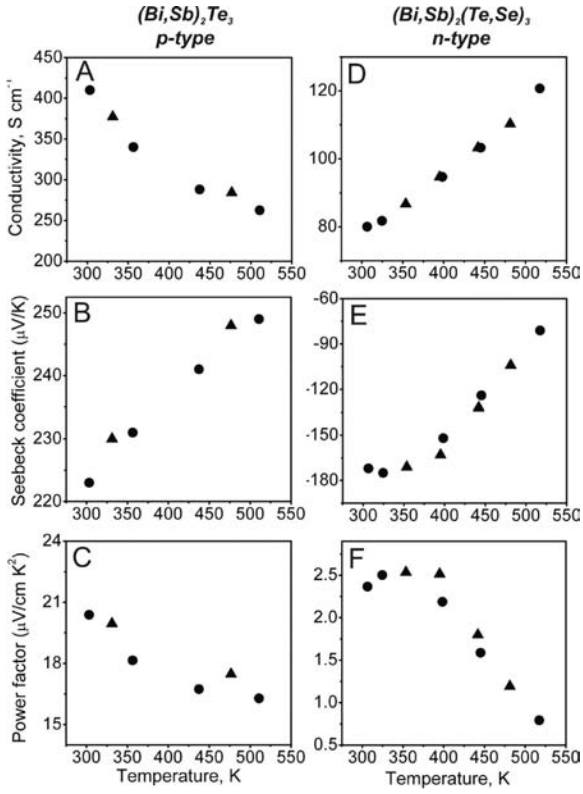

Figure 6. Temperature dependence of the electrical conductivity σ (A, D), Seebeck coefficient S (B, D), and power factor $S^2\sigma$ (C, F), for p-type $(Bi,Sb)_2Te_3$ (A−C) and n-type $(Bi,Sb)_2(Te_{0.9}Se_{0.1})_3$ (D−F). Circles correspond to the forward temperature scan, whereas the triagles represent data points measured during sample cooling.

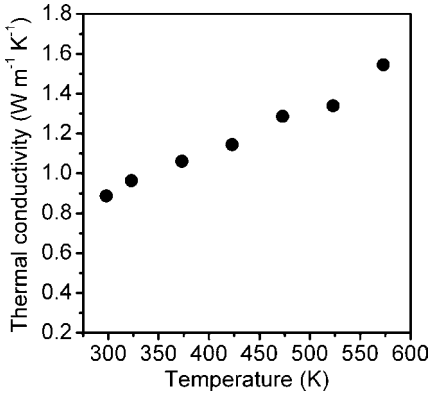

Figure 7. Temperature dependence of thermal conductivity for p-type $(Bi,Sb)_2Te_3$ nanocomposite.

the temperature dependence for thermal conductivity of the nanostructured p-type $(Bi,Sb)_2Te_3$ sample. It was prepared from the NC-ink with a composition identical with that used for the films with electrical properties shown in Figures 6A−C. As expected for a material with nanoscale granularity, we observed significantly lower thermal conductivities (~0.89 W/(m K) at room temperature), as compared to the state-of-the-art commercial BiSbTe ingots ($\kappa \approx 1.4$ W/(m K)).[18,86] The room-temperature κ values of our samples were also lower than that of nanostructured alloys obtained by ball milling and hot pressing of BiSbTe indots ($\kappa \approx 1.1$ W/(m K)).[18] In agreement

(86) Xie, W. J.; Tang, X. F.; Yan, Y. G.; Zhang, Q. J.; Tritt, T. M. *Appl. Phys. Lett.* **2009**, *94*, 102111.

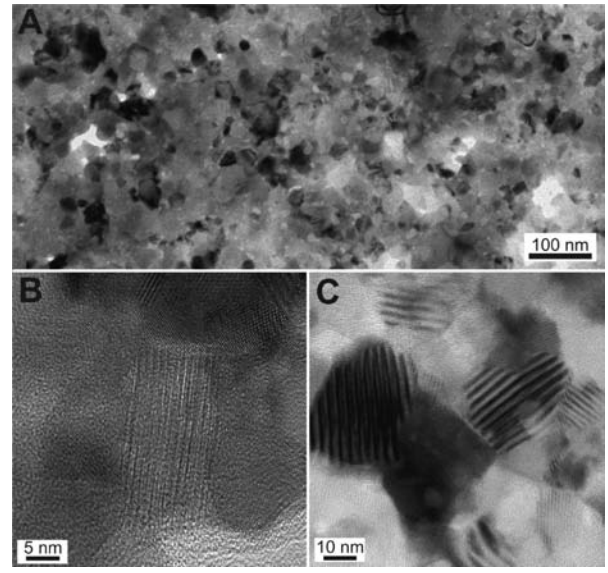

Figure 8. (A) Low- and (B, C) high-resolution TEM images for nanostructured PbTe/$(Bi,Sb)_2Te_3$. The composite was prepared by combining PbTe NCs capped with Sb_2Te_3-MCCs with "$(Bi,Sb)_2Te_3$" ink in a 1:4 molar ratio followed by annealing at 300 °C. Moire fringes on panel C arise from the electron beam diffraction on vertically stacked crystallites.

with other studies of p-$(Bi,Sb)_2Te_3$,[18,86] the thermal conductivity of our samples gradually increased with temperature (Figure 7) due to an increase of lattice phonon conductivity. Significantly lower thermal conductivities were observed in the pellets prepared from the NC-inks and annealed at lower temperatures in Figure S16.[37]

From Figures 6C and 7 we calculated a ZT value of 0.70 at room temperature. This ZT value is higher than previously reported values for solution-processed TE materials.[31,32] Even more important, in contrast to bulk p-type BiSbTe alloys whose ZT drops rapidly with temperature down to about 0.25 at 523 K,[18] ZT values of nanostructured p-$(Bi,Sb)_2Te_3$ prepared from the NC-inks were nearly temperature-independent, with $ZT \approx 0.63$ at 523 K. This notable difference in behavior could originate from the presence of nanosized grains and heterointerfaces. Hot-pressed BiSbTe nanopowders also showed weaker temperature dependence of ZT,[18] suggesting that improved thermoelectric performance of nanostructured p-type $(Bi,Sb)_2Te_3$ phases at elevated temperatures is indeed related to nanostructuring.

Outlook for Further Rational Design of Nanostructured TE Materials. In addition to some obvious routes for further optimization of the materials characteristics such as tuning the carrier concentration, compositional optimizations, control of nanostructuring (e.g., through optimized annealing), and so forth, solution-based fabrication offers further appealing possibilities for materials design. One option is illustrated by TEM images in Figure 8 for a nanocomposite made by combining the previously discussed materials, $(Bi,Sb)_2Te_3$ NC-ink with PbTe NCs capped with Sb_2Te_3-MCCs in a 1:4 molar ratio, followed by annealing at 300 °C. Such a nanocomposite features a broad spectrum of crystallite grain sizes between about 5 and 50 nm (Figure 8A), often with atomically sharp and coherent interfaces (Figure 8B,C). In analogy with biphase PbTe/Sb_2Te_3, immiscibility of PbTe with $(Bi,Sb)_2Te_3$ phases is believed to be an important factor determining nanoscale granularity. Similarly, many other inorganic materials can be added to the NC-inks, allowing the rational design of complex phases and compositions. Furthermore, metallic inclusions can be easily introduced

to the nanocomposites in Figure S17.[37] We may also envision implications of heterostructured (e.g., core−shell) NCs as the building blocks for advanced TE materials.

Conclusions

We have demonstrated that colloidal NCs of lead and bismuth chalcogenides capped with antimony−chalcogenide molecular complexes can serve as precursors for designing nanostructured thermoelectric materials. This new methodology shows a set of advantages such as all-inorganic design, nanostructuring, compositional flexibility, and possibility of solution deposition using conventional techniques (spray coating, spin casting). Two distinctly different concepts for the material formulation were explored. The first concept preserves the benefits of nanostructuring and quantum confined semiconductors and allows examining the effect of quantum confinement on the thermopower and other characteristics. This was demonstrated for solids composed of PbTe NCs capped with Sb_2Te_3-MCCs, exhibiting a record for PbTe values of thermopower ($S \approx 750\ \mu$V/K), while the conductivities are still lower than those required to meet practical applicability of the material. The second concept does not preserve the NC integrity but instead uses colloidal NCs for nanoscale solid-state chemical transformations leading to desired TE compounds. We fabricated alloyed single-phase $(Bi,Sb)_2Te_3$ and two-phase $PbTe/Sb_2Te_3$ nanostructured thin films by combining and reacting Bi_2S_3 or PbS NCs with Sb_2Te_3 molecular precursor in hydrazine. p-type $(Bi,Sb)_2Te_3$ and n-type $(Bi,Sb)_2(Te_{0.9}Se_{0.1})_3$ exhibited high Seebeck coefficients of $\pm 200-250\ \mu$V/K and conductivities up to 450 S cm^{-1}, closely approaching values required for commercial applications. Thus, high power factors up to 20.4 μW cm^{-1} K^{-2} and *ZT* values of 0.7 were obtained.

Acknowledgment. We thank P. Guyot-Sionnest, E. Shevchenko, and D. Mitzi for stimulating discussions, R. Jaramillo for a help with low-temperature conductivity measurements, D. Shepard (Netzsch Instruments North America, LLC) for thermal conductivity measurements, M. Bodnarchuk for synthesis of Au NCs, S. Rupich for reading the paper, and the Analytical Chemistry Laboratory at Argonne National Laboratory (ANL) for elemental analysis. The work was supported by Evident Technologies, Inc., and NSF CAREER under Award No. DMR-0847535. The work at the Center for Nanoscale Materials (ANL) was supported by the U.S. Department of Energy under Contract No. DE-AC02-06CH11357.

Supporting Information Available: Text and figures giving additional experimental details. This material is available free of charge via the Internet at http://pubs.acs.org.

JA909591X